CONF-790420--20

HEDL-SA-1675 FP

MASTER

HELIUM BUBBLES IN IRRADIATED BORON CARBIDE

GW Hollenberg
B Mastel

81st Annual Meeting of the American Society Ceramic, Cincinnati, Ohio
April 28-May 2, 1979

HANFORD ENGINEERING DEVELOPMENT LABORATORY
Operated by Westinghouse Hanford Company, a subsidiary of Westinghouse Electric Corporation, under the Department of Energy Contract No. EY-76-C-14-2170

DISCLAIMER

HEDL-SA-1675-A

HELIUM BUBBLES IN IRRADIATED BORON CARBIDE

By

G. W. Hollenberg
B. Mastel

ABSTRACT

Boron carbide, in nuclear reactor neutron absorber applications, generates large quantities of helium, some of which is trapped in small bubbles within the grains. Transmission electron microscopy was used to examine the size distribution, shape and density of these bubbles in boron carbide irradiated to temperatures between 540°C and 2000°C to burnups between 27 and 62x10^{20} captures/cm^3.

ACKNOWLEDGMENTS

Most of the irradiated material examined in this investigation was obtained from experimental subassemblies which were designed, constructed and irradiated under the cognizance of J. A. Basmajian.

Figures 1 and 2 are the products of previous work by D. E. Mahagin, W. V. Cummings and J. J. Laidler.

HELIUM BUBBLES IN IRRADIATED BORON CARBIDE

G. W. Hollenberg and B. Mastel

1.0 INTRODUCTION

Boron carbide has been internationally accepted as the neutron absorber material for use in fast neutron reactors. Its availability and high reactivity-worth in safety and control rod applications has led to these applications. In the course of experimentally establishing the range of conditions (i.e., temperature, burnup, etc.) in which boron carbide performance is adequate, sample pellets have been retrieved and examined with the transmission electron microscope. The investigation reported here is a review of examinations on boron carbide with burnup levels to 62×10^{20} captures/cm^3 and irradiation temperatures from 540 to 2000°C.

Boron carbide absorbs neutrons by the following reaction in which lithium and helium are formed:

$$^{10}B + {}^{1}n \rightarrow {}^{7}Li + {}^{4}He$$

Hence, burnup values, besides indicating the number of ^{10}B atoms missing, also describe the amount of helium and lithium produced in the lattice. Helium is a gas which is expected to have insignificant solubility in the ceramic matrix. Two paths out of the crystal lattice are possible for the helium atoms that are generated. They can diffuse through the crystallites to a free surface where they produce a buildup of control pin plenum pressure. Alternatively, the helium atoms can precipitate into internal pockets within the crystallites. This in turn is thought to produce swelling in the boron carbide. Both the pellet swelling and gas pressure in the pin plenum limit the useful lifetime of absorber elements since each can cause excessive stress in the cladding and consequently, increase the potential for a cladding rupture. Hence, the mechanism by which these nuclear reaction products are accommodated in the boron carbide structure is important, because it is related to the two major design criteria applied to the boron carbide pellets: helium release and swelling.

Transmission electron microscopy investigations of irradiated boron carbide have consistently revealed small platelike cavities or bubbles [1-7] on the {110} or {111} rhombohedral planes. These cavities were presumed to be filled with high-pressure helium, since strain fields were observed in the immediate vicinity, see Figure 1. Hollenberg, et al. [6] suggested that the bubbles were responsible for crystallite swelling in the direction normal to the bubbles. Hollenberg, et al., also concluded that anisotropic crystallite swelling was the driving force for intergranular microcracking. Only in the latter investigation was material examined with more than 50×10^{20} captures/cm^3. A systematic investigation of the influence of temperature on the helium bubbles has not been reported.

Postirradiation annealing experiments at high-temperatures ($T > 1200°C$) have been conducted by two sets of investigators. [2,7,8] In both cases, annealing at temperatures near 1800°C resulted in stress relaxation around the bubbles as the result of an increase in bubble size and the adoption of a more equilibrium (that is, more equiaxed) shape, see Figure 2. Both sets of investigators suggested that such bubbles might be formed in-reactor if irradiation temperatures were to reach these levels.

To place a perspective on helium retention in boron carbide consider the balloon in Figure 3. If the pellet pictured in Figure 3 were to retain 80% of the helium produced (a typical value), then 900 cc (STP) or approximately 50,000 ppm, would be compressed into tiny bubbles within the pellet. Comparing this to the amount of helium implanted in the investigation of irradiation effects on metals (50 to 4000 ppm) [9-11] reveals the massive amount of helium that can be retained by boron carbide.

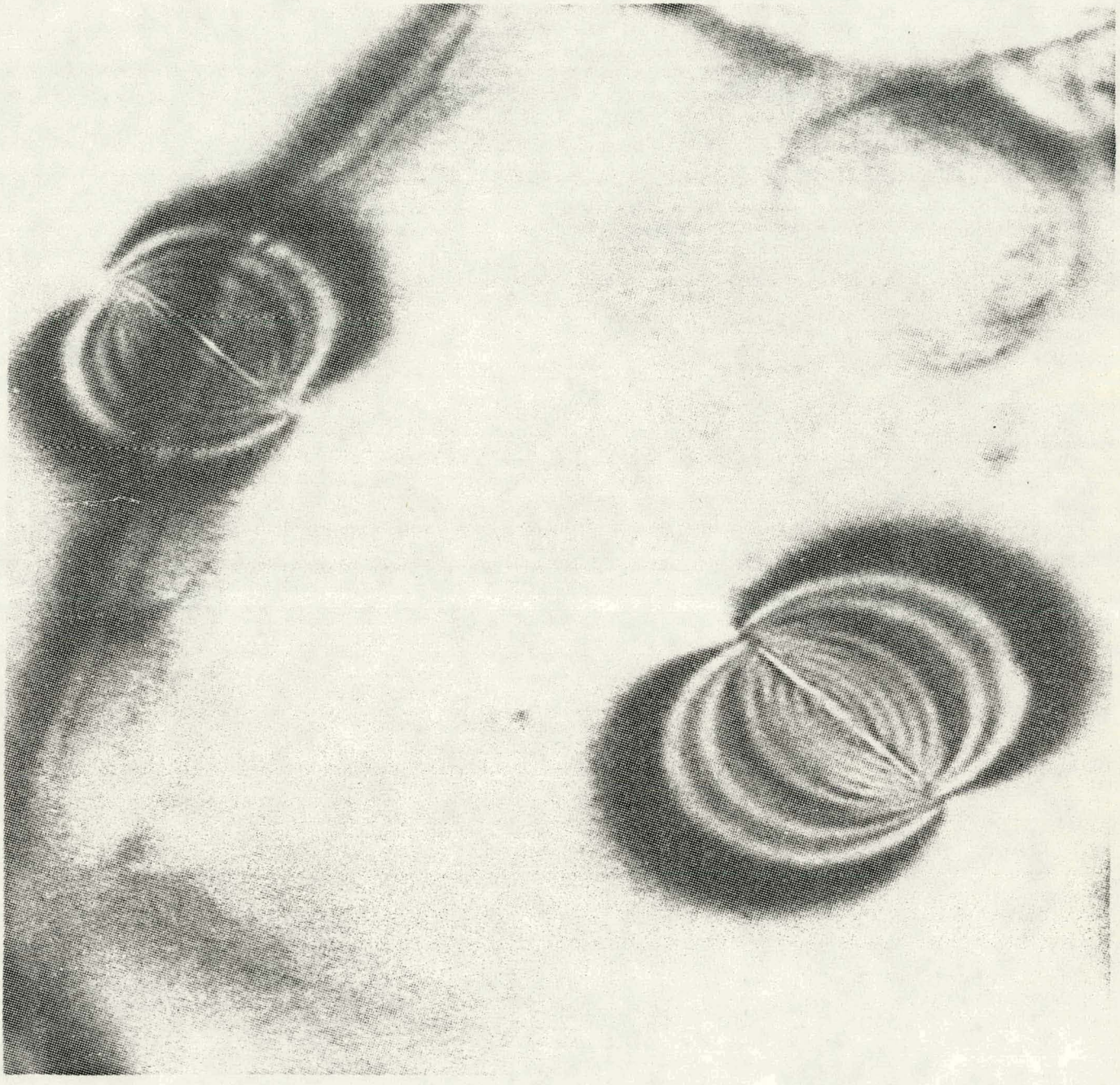

HEDL 7901-186.13

FIGURE 1. Strain Fields Surrounding Bubbles in Low Burnup Boron Carbide (11×10^{20} Captures/cm^3). (Reference 1)

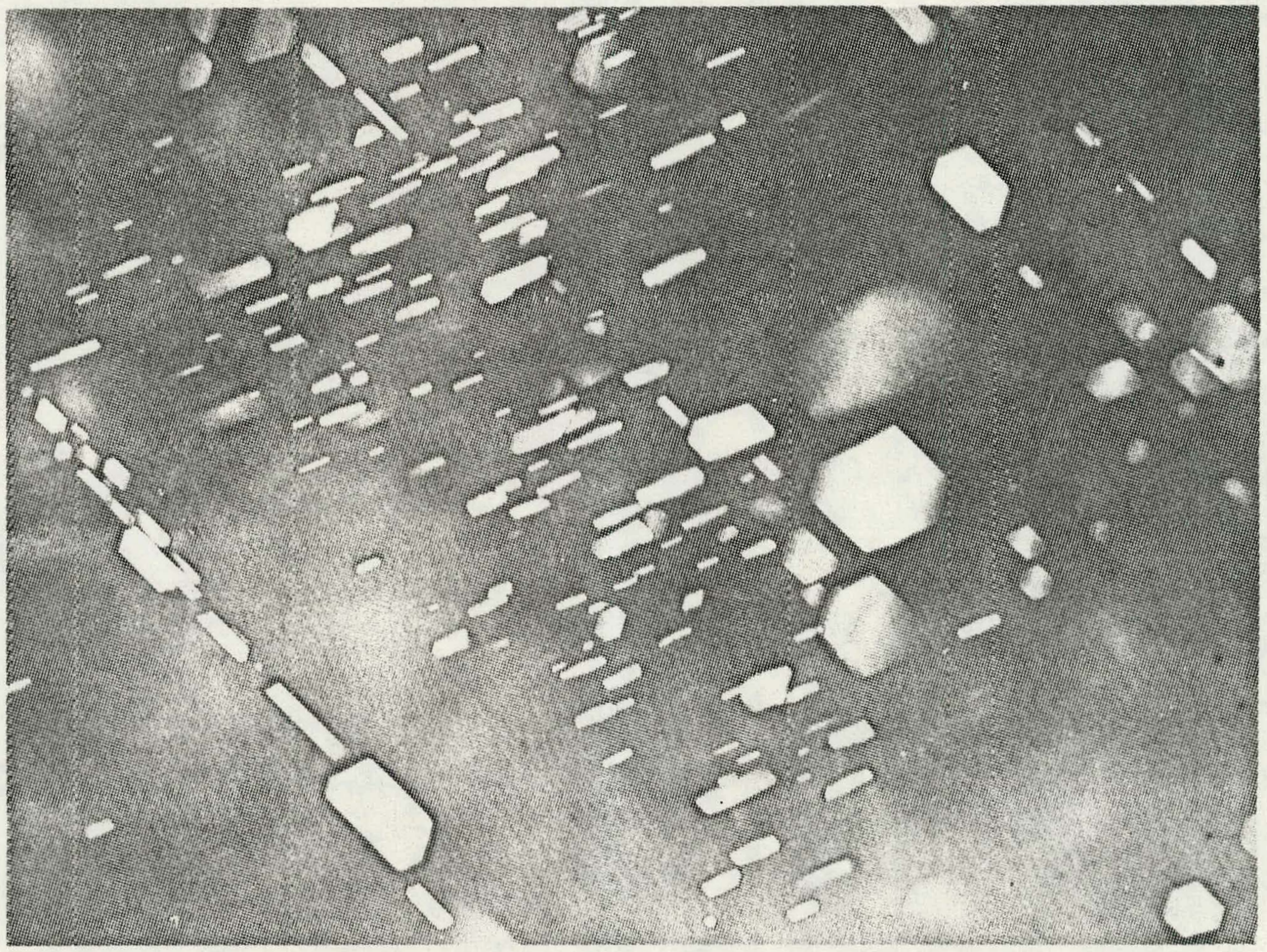

FIGURE 2. Effect of Annealing on Bubbles in Low Burnup Boron Carbide. Irradiated at 800°C to 11×10^{20} Captures/cm^3, but Annealed After Irradiation at 1800°C for 5 Hours. (Reference 8) HEDL 7901-186.11

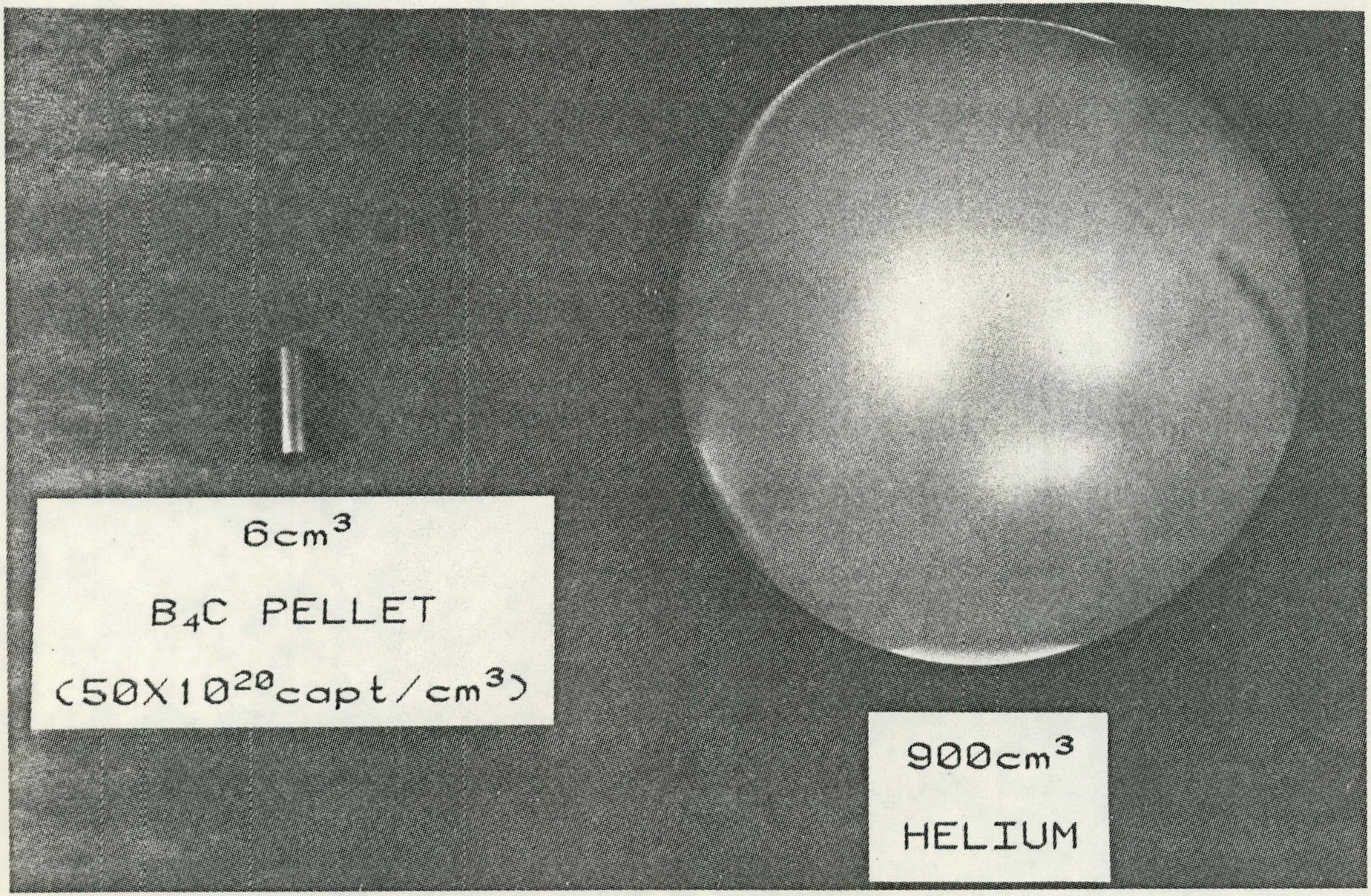

FIGURE 3. Helium Retained in Boron Carbide Irradiated at 50×10^{20} Captures/cm^3.

Materials and Irradiation

Irradiated specimens were obtained from experimental subassemblies irradiated in the EBR-II reactor. The general irradiation and experimental conditions have been previously described.[12] Polycrystalline boron carbide pellets were encapsulated in stainless steel tubing and irradiated in the high-energy neutron environment of EBR-II, with at least 50% of the neutrons expected to possess energies above 0.1 MeV. The starting pellets were hot-pressed to 92% of theoretical density from essentially stoichiometric boron carbide powders ($B_{4.1}C$ to $B_{3.9}C$). The ^{10}B isotopic content of the boron was increased from that of natural boron to 92% ^{10}B so as to increase the rate of burnup. The average grain size ranged from 3 to 20 μm, but was approximately 10 μm for most of the specimens. During irradiation, pellet centerline temperatures were between 540 and 2000°C. Centerline temperatures were predicted from thermal analysis.[12] Ultimate burnup levels were determined from plenum pressures and helium released during postirradiation melting of pellets. Samples were selected for viewing such that final burnup levels varied between 27×10^{20} and 62×10^{20} captures/cm^3, with most of the samples possessing a burnup of approximately 50×10^{20} captures/cm^3.

Transmission Electron Microscopy

Many specimens were simply cut from the pellets with a diamond saw and then polished as thin as practical (2 mils). The thin discs were further thinned by argon ions in preparation for viewing by a transmission electron microscope. Care was taken to extract a 3 mm diameter TEM disc from the center of the pellet. Because of the friable nature of most of the samples, mechanical operations were held to a minimum.

Other specimens were so friable after irradiation that it was not possible to prepare and view an ion milled cross section. From these pellets, a small quantity of the material was powdered by a mortar and pestle to less than 100 mesh. The irradiated powder was then mixed with aluminum powder. The mixture was pressed into a 3 mm diameter disc at 470°C under a pressure excess of 30,000 psi. The disc was then prepared for viewing in the electron microscope in the same manner as a conventional disc.

Samples were examined with a Phillips 100 microscope operated at 100 KV, As shown in Figure 1, the strain fields can accentuate single bubbles. When viewing a high density of bubbles, these same strain fields make interpretation difficult; hence, absorption contrast was preferred. In the interest of conserving time, the scope of this investigation was intentionally limited to bubble size, shape and density determinations, and sidelights such as bubble orientation, strain levels, etc., were ignored.

Micrographs

In Figure 4, a transmission electron micrograph of boron carbide irradiated at 540°C to 50×10^{20} captures/cm^3 is shown. The lenticular bubbles, were quite small with major diameters that did not exceed 0.03 μm and an average bubble diameter that was perhaps less than 0.005 μm. In the low temperature samples, these small bubbles were observed to be homogeneously distributed throughout the crystallites with the exception of a narrow depletion region near grain boundaries. Many of the bubbles were at the resolution limit of this microscope ($\sim$ 0.005 μm). It is logical to expect a continuous spectrum of bubble sizes, which would imply that there were numerous bubbles smaller than the resolution limit. The bubble height (the minor axis) was so small that it could not be resolved.

In Figure 5, a transmission electron micrograph of boron carbide irradiated at 900°C to 50×10^{20} captures/cm^3 is shown. At this slightly higher temperature, the bubbles still retained a lenticular shape. A few bubbles were much larger than the rest, about 0.1 μm in length. Note that the smaller bubbles were not formed in the region adjacent to the larger bubbles. Elsewhere, the smaller bubbles were homogeneously distributed.

Figure 6 shows a transmission electron micrograph of boron carbide that was irradiated at a maximum temperature of 1050°C for 62×10^{20} captures/cm^3 in an instrumented absorber experiment. The spectrum of observable bubbles sizes increased such that bubble diameters ranged all the way from 1 μm down to the resolution limit of the microscope ($\sim$ 0.005 μm). As in the material irradiated at 900°C (Figure 5), the boron carbide displayed in Figure 6 exhibited an absence of the smaller bubbles near the larger bubbles. It appeared that the height (minor axis)

FIGURE 4. Small Lenticular Bubbles in Boron Carbide Irradiated at 540°C to 50×10^{20} Captures/cm^3.

HEDL 7901-186.1

FIGURE 5. Lenticular Bubbles in Boron Carbide Irradiated at 900°C to 50×10^{20} Captures/cm^3.

HEDL 7901-186.2

FIGURE 6. Large Lenticular Bubbles in Boron Carbide Irradiated at a Maximum Temperature of 1050°C for 62×10^{20} Captures/cm^3.

HEDL 7901-186.4

of the bubbles also increased at this higher temperature, such that the aspect ratio of the bubbles was reduced. Except for the localized depletion around large bubbles, the distribution of bubbles, both large and small, appeared to be uniform throughout the crystallites.

At 1500°C (but a somewhat lower burnup, 36×10^{20} captures/cm^3), the bubbles became heterogeneously distributed, as seen in Figure 7. In Figure 7, a set of bubbles is featured near the center but the remaining area is void of bubbles. Throughout this material, bubbles were observed to be concentrated in a grain surrounded by grains devoid of bubbles.

The bubbles in the boron carbide irradiated at 1500°C were generally larger than their lower temperature counterparts. It should be noted in Figure 8 that many of these bubbles were not lenticular, but had a more equiaxed shape with faceted sides. The faceted bubbles closely resembled those produced by post-irradiation annealing (compare Figures 8 and 2).

In Figure 9, boron carbide irradiated at a predicted temperature of 2000°C to a burnup of 27×10^{20} captures/cm^3 possessed faceted bubbles at high magnification. The heterogeneous character of these small bubbles is emphasized in Figure 10, where a string of bubbles was observed in a grain. The faceted bubbles were perfectly aligned and appeared to completely traverse the crystallite. In Figure 11, another string of these small faceted bubbles is shown in contrast with associated dislocations. Many of these bubble strings were observed in the higher temperature samples, and all appeared to have dislocations nearby. Almost all of the small diameter bubbles ($d < 0.1$ μm) were in linear arrays.

A lower magnification photomicrograph of the boron carbide irradiated at 2000°C, Figure 12, depicts larger bubbles. Note the presence of both low and high aspect ratio bubbles in this area. Note the large number of dislocations near the bubbles and apparent stacking faults. In Figure 13, dislocations

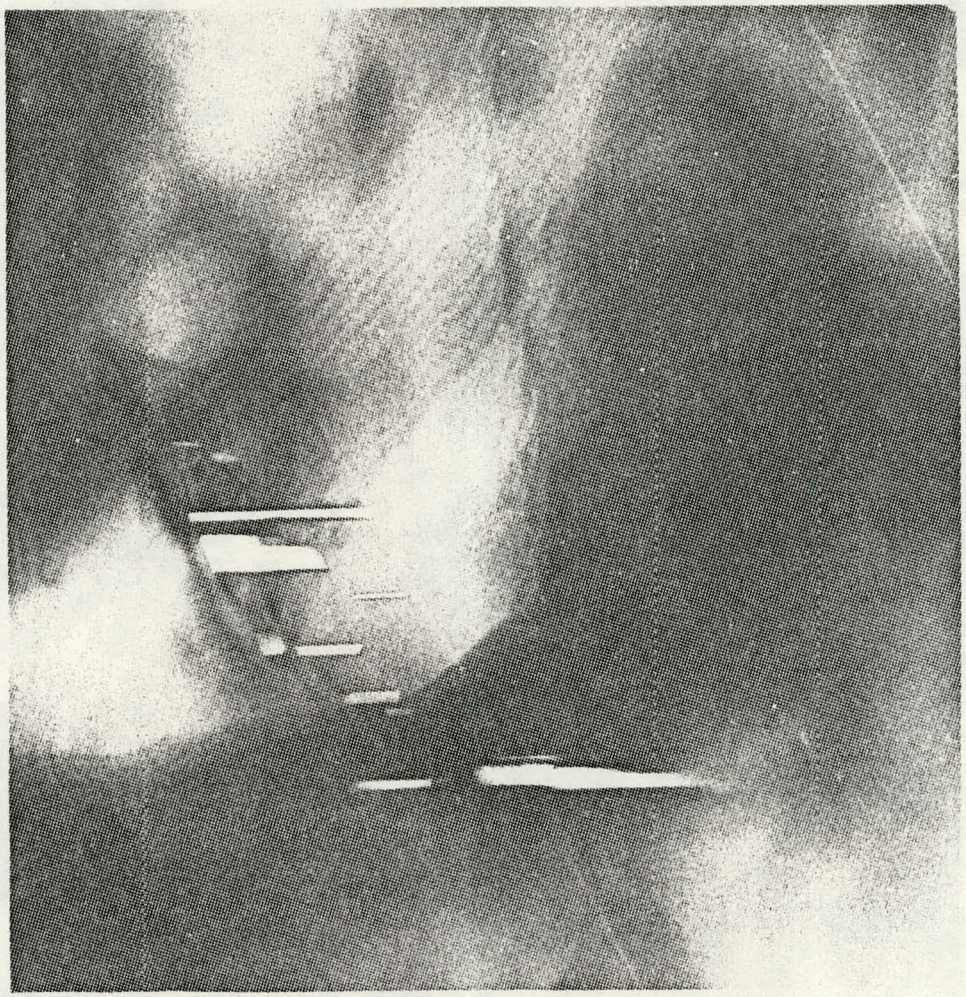

FIGURE 7. Faceted Bubbles in Boron Carbide Irradiated at 1500°C to 35×10^{20} Captures/cm^3.

HEDL 7901-186.12

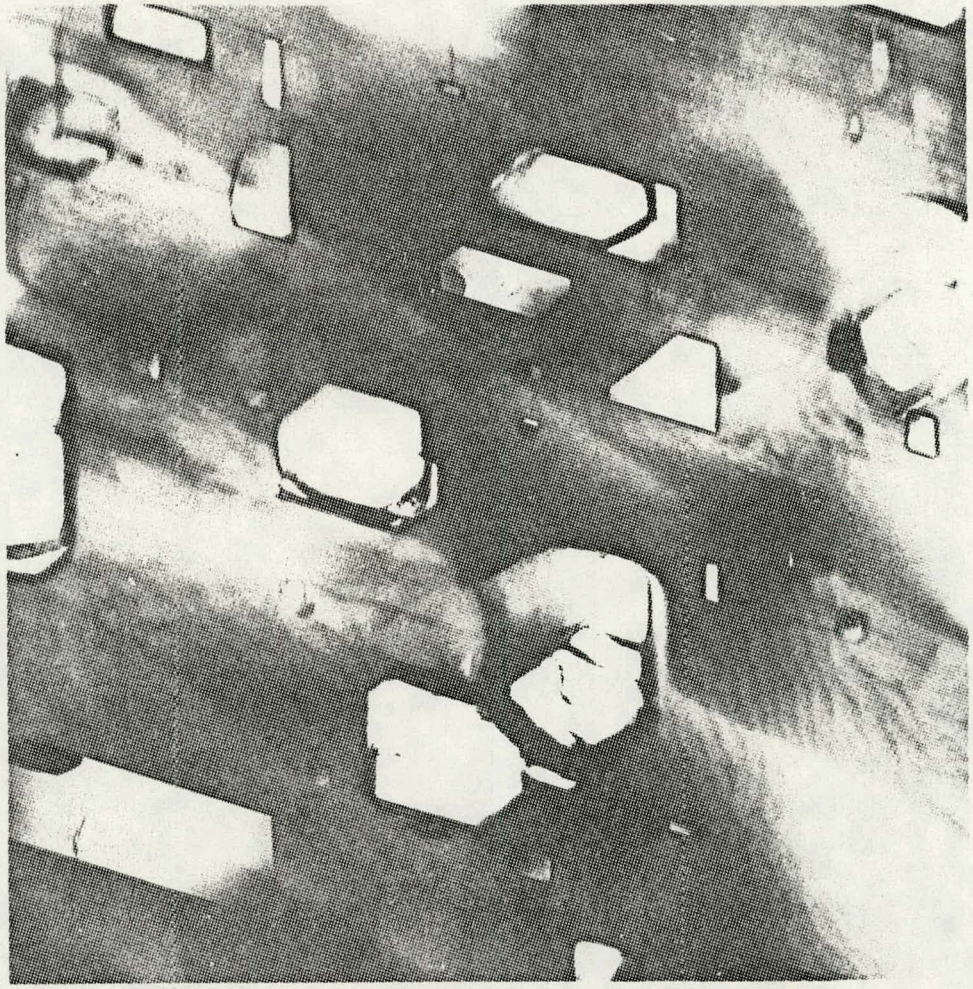

FIGURE 8. Faceted Bubbles in Boron Carbide Irradiated at 1500°C to 35×10^{20} Captures/cm^3.

HEDL 7902-041.3

FIGURE 9. Faceted Bubbles in Boron Carbide Irradiated at 2000°C.

HEDL 7901-186.5

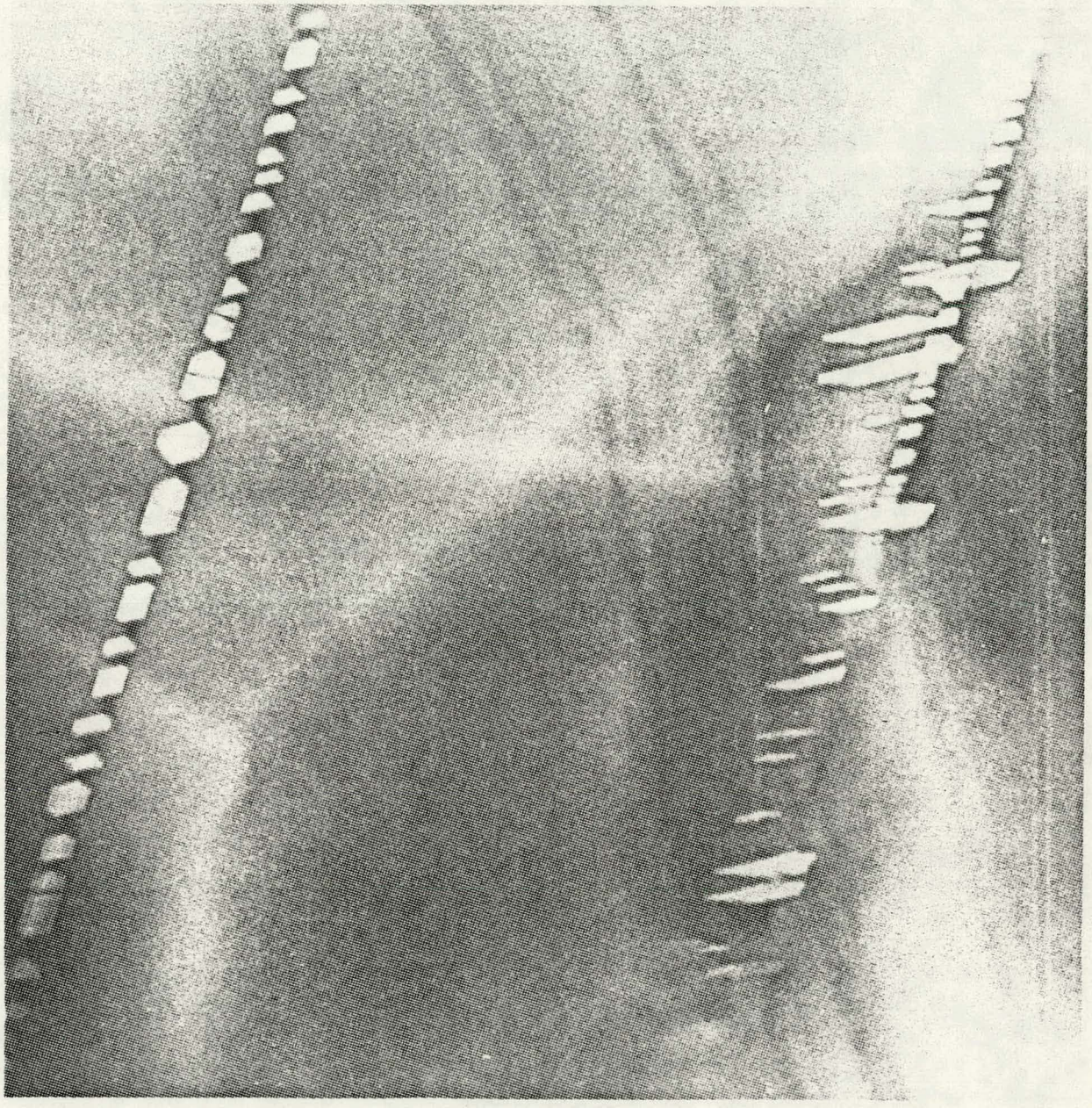

FIGURE 10. String of Bubbles in Boron Carbide Irradiated at 2000°C.

HEDL 7901-186.9

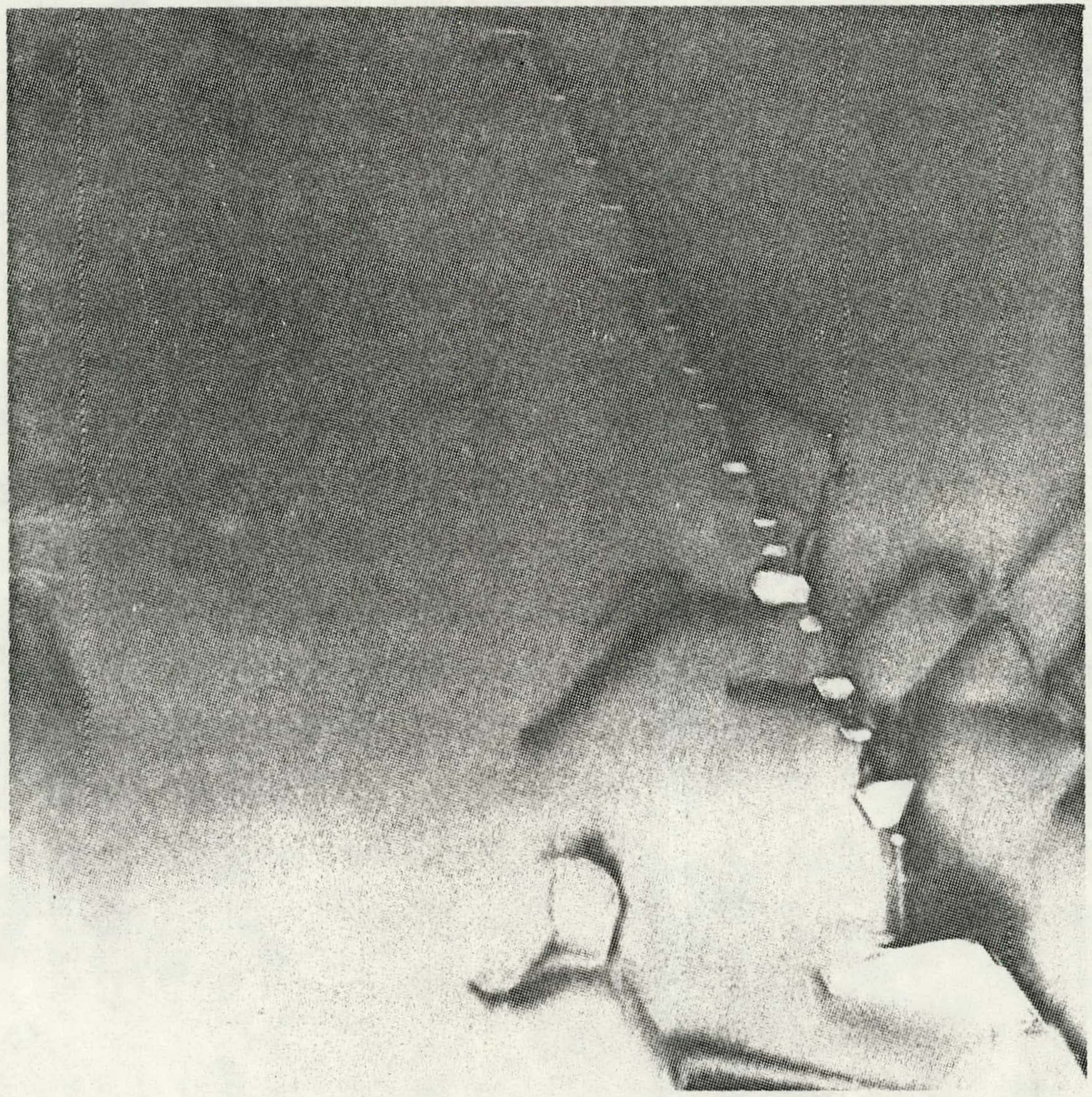

HEDL 7902-196.1

FIGURE 11. A String of Bubbles With a Dislocation in Boron Carbide Irradiated at 2000°C.

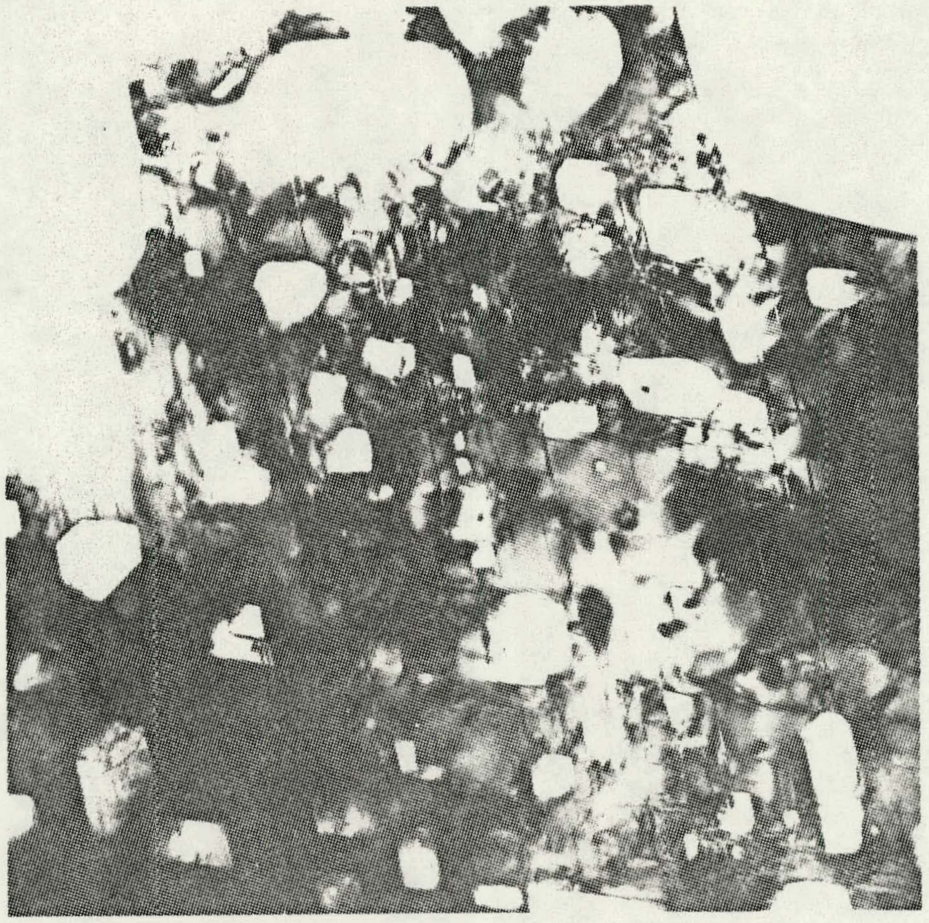

FIGURE 12. Large Faceted Bubbles in Boron Carbide Irradiated at 2000°C With Dislocation Array.

HEDL 7901-186.6

appeared to parallel the faceted sides of the bubbles and complex stress patterns were developed. An even lower magnification photomicrograph (Figure 14) displayed even larger bubbles (3 μm). Also, note that many bubbles were associated with grain boundaries. Realizing that all samples originally possessed 8% porosity, one must conclude that some of the voids were not irradiation induced, but were residual porosity. Differentiation is difficult, but porosity in virgin boron carbide tends to form at triple points, like the one just above the center of the photograph.

In addition to bubbles located on dislocation and grain boundaries, it was observed that the twins, which are quite common in hot-pressed boron carbide, had bubbles starting at their boundaries in the high temperature material. In Figure 15, bubbles traversed a twinned region in the interior of a boron carbide grain which has been irradiated at 1500°C.

Before considering quantitative aspects of the bubbles in irradiated boron carbide, the qualitative observations should be reviewed. As depicted in Figure 16, the following generalizations can be made:

1. Low Temperatures ($T < 900°C$)
   a. Small bubbles (0.01 μm)
   b. High bubble density
   c. Homogeneous bubbles
   d. Lenticular shape

2. High Temperatures ($T \geq 1500°C$)
   a. Large bubbles (1.0 μm)
   b. Low bubble density
   c. Heterogeneous bubbles
   d. Equiaxed and faceted bubbles

At temperatures between the extremes of 540 and 2000°C there appeared to be a progression in bubble size, shape and density.

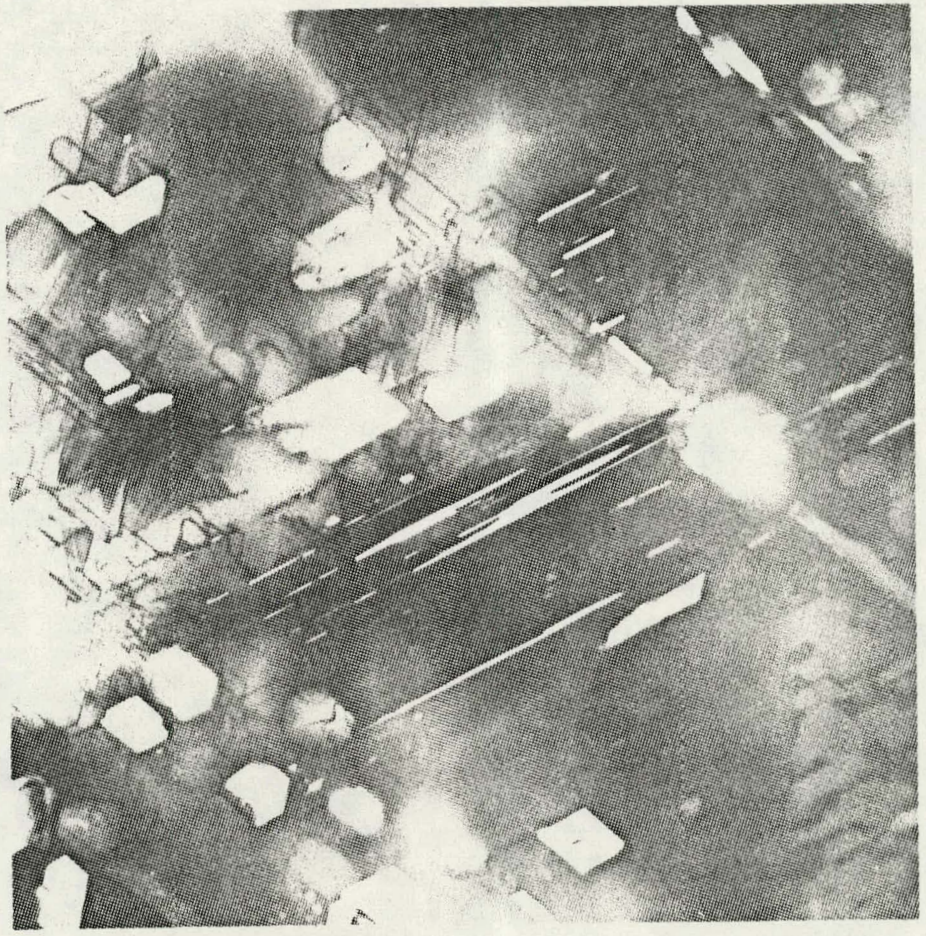

FIGURE 13. Large Faceted and Lenticular Bubbles in Boron Carbide Irradiated at 2000°C.

HEDL 7901-186.8

HEDL 7901-186.7

FIGURE 14. Large Bubbles on Grain Boundaries of Boron Carbide Irradiated at 2000°C.

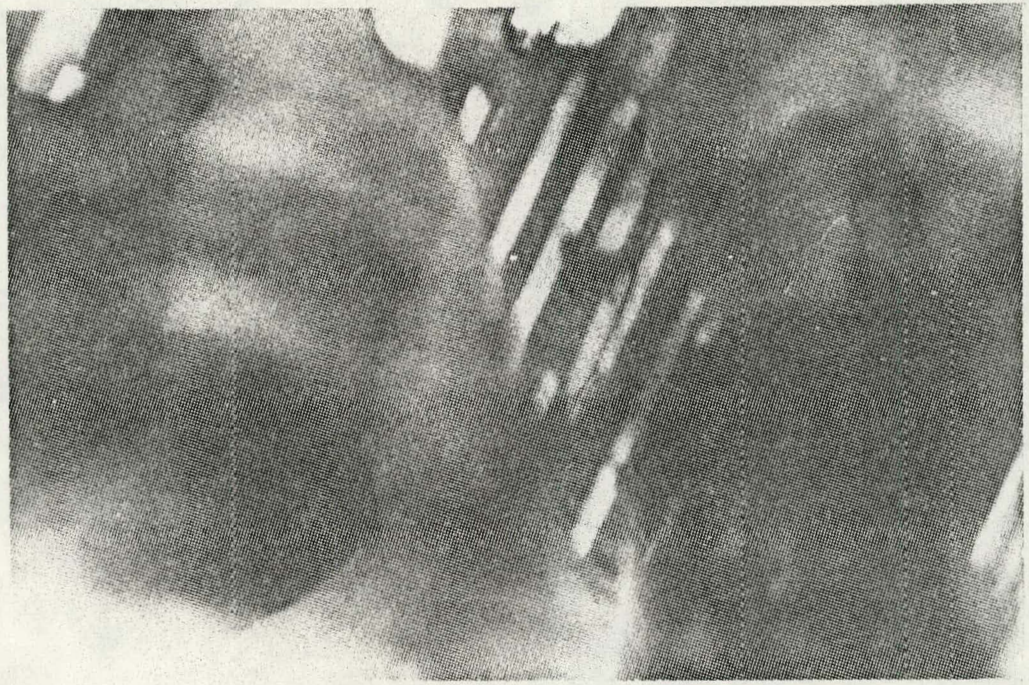

Figure 15. Bubbles Located in Twinned Region of Boron Carbide Irradiated at 1500°C.

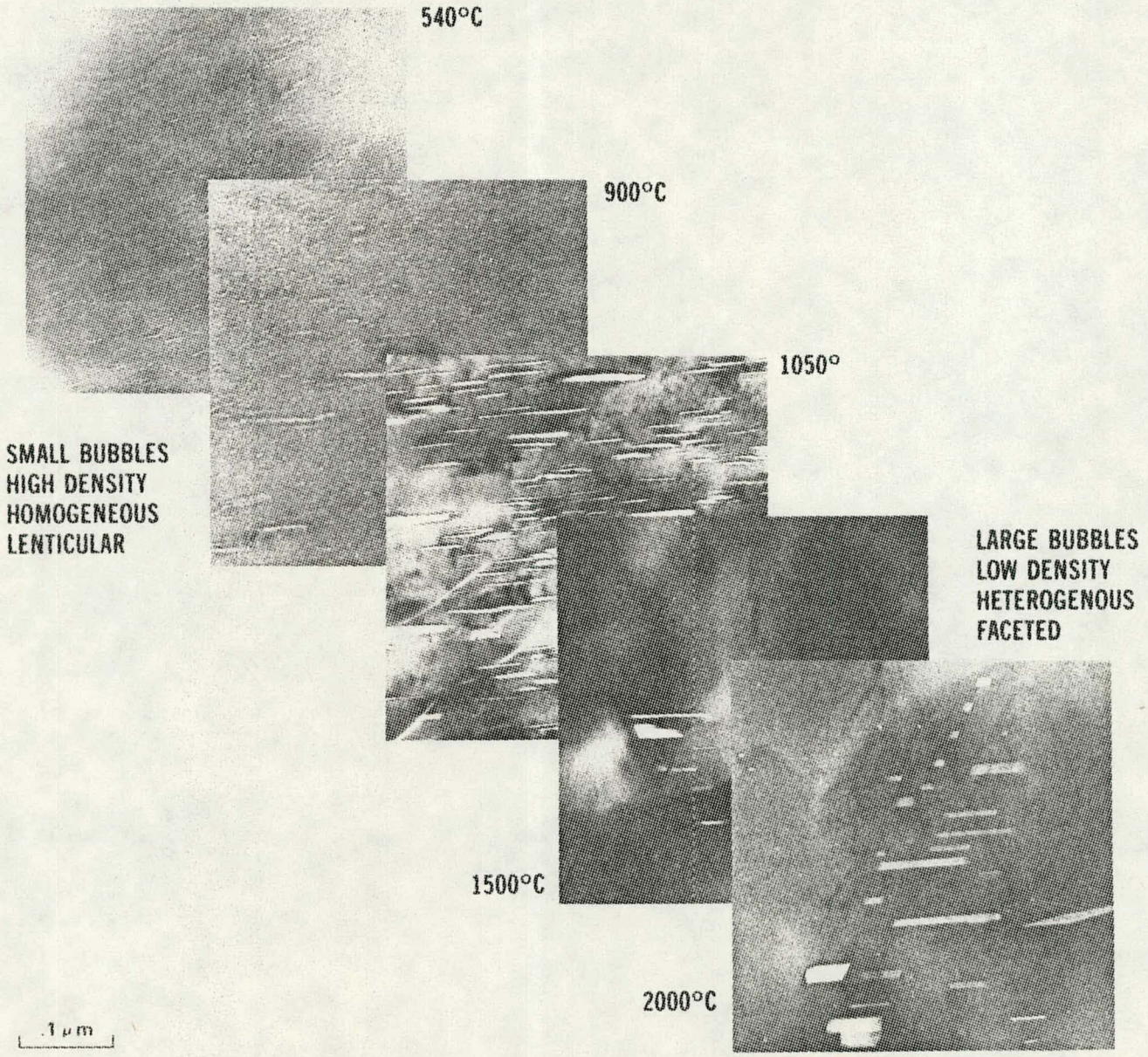

FIGURE 16. The Effect of Temperature on Bubbles in Irradiated Boron Carbide.

HEDL 7902-62

Quantitative Evaluation

Two parameters, bubble density and diameter, were used to quantitatively characterize the changes in bubbles as irradiation temperature increased. To obtain representative values for each sample, 900 bubbles were counted. Other parameters such as bubble shape and homogeneity did not lend themselves to quantitative assessment.

To determine the bubble density, $\overline{\rho}$, in the irradiated boron carbide the following relationship was used:

$$\overline{\rho} = \sum_{i=0}^{i=\infty} \frac{n_i}{A \cdot T} \qquad \text{Eq. 1}$$

where A was the foil area considered and T was the foil thickness. The foil thickness was obtained by viewing stereo pairs taken at greater than 12° apart. By focusing on the uppermost and then the lowest features in the foil, it was possible to measure the vertical distance between them. This distance was used as the foil thickness. Foil thickness varied between .01 and 1 μm in most areas considered.

In Equation 1, n_i represents the number of bubbles measured to be of size d_i in diameter. Almost all of the bubble counting was done with a Carl Zeiss Particle Size Analyzer. Using the analyzer, d_i represented the major dimensions of the high aspect ratio lenticular bubbles and the largest dimension of the more equiaxed bubbles that occurred at higher temperatures. The analyzer partitioned bubbles into 48 different size groupings from 1 to 26 mm on the magnified photographs.

The effective bubble diameter, $\overline{d}$, was determined from the averaged bubble volume, $\overline{V}$:

$$\overline{d} = \left(\frac{\overline{V}}{K}\right)^{1/3}$$

where K is a geometric factor which was assumed constant. $\overline{V}$ was determined from the following expression:

$$\bar{V} = \frac{\sum_{i=0}^{i=\infty} n_i V_i}{\sum_{i=0}^{i=\infty} n_i} = \frac{\sum_{i=0}^{i=\infty} n_i K (d_i)^3}{\sum_{i=0}^{i=\infty} n_i} \qquad \text{Eq. 2}$$

Multiple photographs were used to characterize different areas in each sample, sometimes with differing magnification. Low temperature samples were always photographed at high magnifications; and consequently, overall bubble densities and diameters were simply averages of all the values from the photographs.

Material irradiated at high temperature possessed such a spectrum in bubble size (almost 3 orders of magnitude) that both high (300,000X) and low (5000X) magnification photographs were necessary. Obviously, one large bubble (1 μm) would fill a high magnification micrograph by itself, and yet, small bubbles (d_i < 0.1 μm) could not be resolved at low magnification. In these cases, only bubbles less than 0.1 μm were counted on high magnification micrographs while only bubbles greater than 0.1 μm were counted on the low magnification micrographs. The average bubble density was then computed by considering the two populations together, hence,

$$\bar{\rho} = \bar{\rho}_L + \bar{\rho}_S$$

where $\bar{\rho}_L$ and $\bar{\rho}_S$ were the large and small bubble densities, respectively. Also, the average volume became,

$$\bar{V} = \frac{\bar{V}_L \bar{\rho}_L + \bar{V}_S \bar{\rho}_S}{\bar{\rho}}$$

where $\bar{V}_L$ and $\bar{V}_S$ were the average bubble volumes for large and small bubbles, respectively.

There are several sources of error expected in these measurements. Since orders of magnitude changes in size and density were apparent in these samples the impact of these errors was not as severe as it might otherwise have been.

Heterogeneity, especially in the high-temperature samples, can introduce error into these results. An effort to select representative photographs was made; but it is believed that there was a tendency to photograph areas with more uniform etching and higher bubble concentrations rather than less aesthetic areas. When large bubbles were present, complete exclusion of initial porosity was difficult.

The finite specimen thickness which was required for viewing induced a positive bias to bubble density measurements, since bubbles without their centers in the foil thickness were included in the counting process. [13] In addition the truncation of the larger bubbles by the top and bottom surface influenced the observed bubble diameters.[13]

At low temperatures, the small bubbles sizes measured (0.004 μm) suggested that even smaller bubble sizes existed. Resolution by the microscope precluded the inclusion of these smaller bubbles in the population. Obviously, the resolution limit influences the accurate measurement of these small bubbles.

In order to evaluate the influence of temperature on bubbles, the data were treated as if all the samples were irradiated at the same burnup; a convenience not available in the reality of multiple irradiation experiments. Most sample burnups were between 48 and 62×10^{20} captures/cm^3; but the high temperature samples possessed lower values (27 to 35×10^{20} captures/cm^3). There is no basis to expect decreases in bubble size or dramatic changes in bubble density at higher burnup levels in these high temperature samples.

In Figure 17, the effective bubble diameter is plotted against irradiation temperature. The error bar on each data point represents the span of observed bubble diameters observed. As anticipated from viewing the micrographs, the bubble diameter increased with temperature. At low temperature the average bubble diameters approach the resolution limit of the microscope; the minimum is certainly smaller than this limit.

Although the average diameter does not increase appreciably between 540 and 1000°C, the maximum bubble diameter does. Above 1000°C, not only did the maximum bubble size increase with temperature, but also the average bubble size increased to over 1 μm. In addition, very small bubbles (d < .01 μm) were not observed in the high temperature samples. Within the resolution range of the microscope, the distribution of bubble diameters appeared to broaden at higher temperatures.

In Figure 18, bubble density is plotted against temperature. The bubble density appeared to be inversely related to the average bubble diameter. At low temperatures (T < 1000°C) the bubble densities were approximately 10^{17} to 10^{18} bubbles/cm^3. At higher temperatures (2000°C) it dropped to 10^{12} bubbles/cm^3. Mahagin[8] also reported bubble densities of 10^{17} to 10^{18} at a much lower burnup level (15×10^{20} captures/cm^3) in the lower temperature range (700°C).

Discussion

Theories specifically developed for helium bubble formation in boron carbide are not available. In nuclear fuels, however, concern with the fate of fission produced gases dates back to the 1950's. Since then myriad mechanisms have been proposed, but their application to boron carbide has been limited.[14] In these theories, the major mechanistic processes that have been considered are:

1. Gas Production
2. Nucleation
3. Bubble Growth
   - Diffusion
   - Coalescence
   - Resolution
4. Bubble Migration
5. Interaction with Lattice Defects

Each of these processes will be considered in light of the data available for helium in boron carbide.

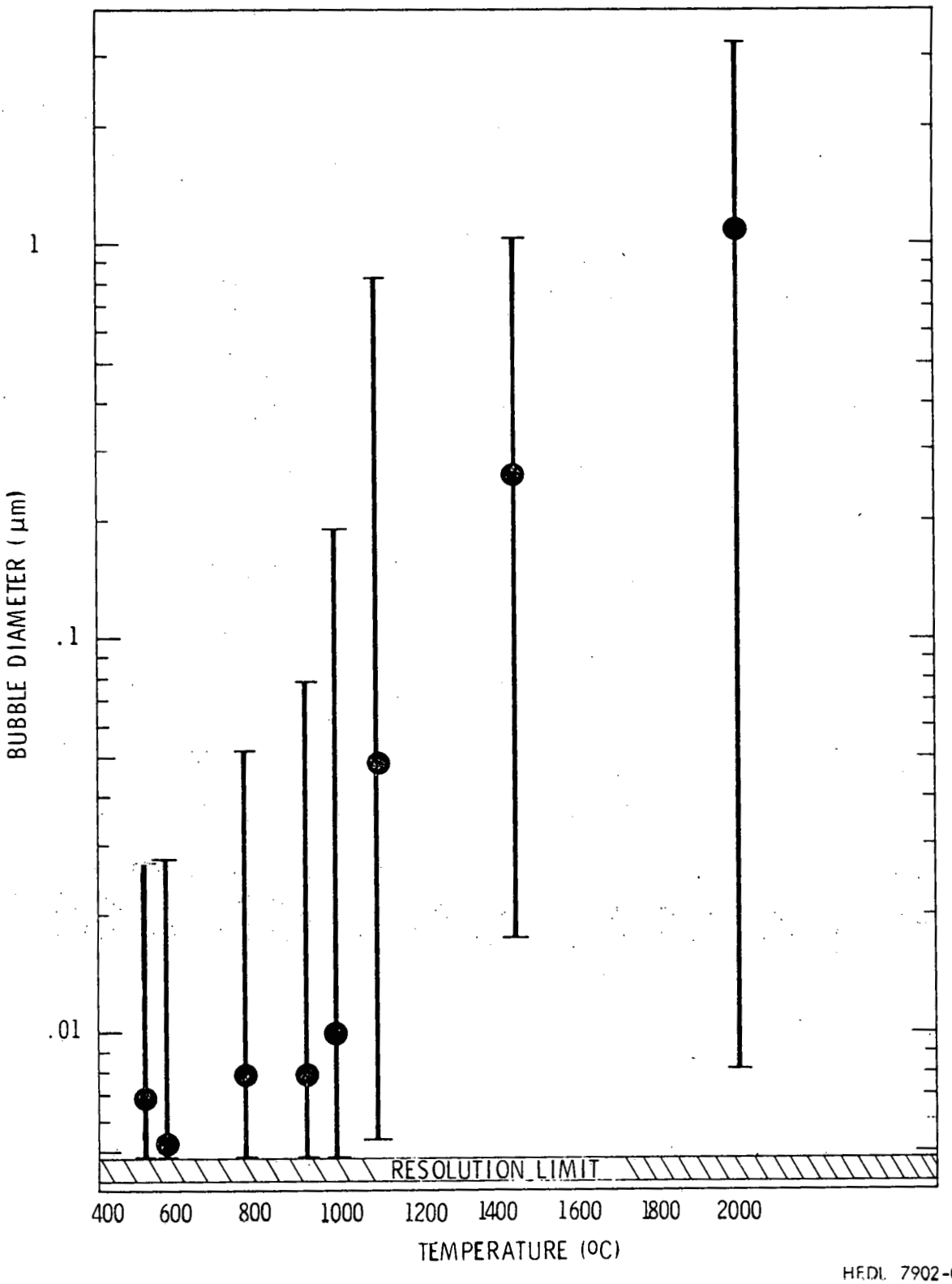

FIGURE 17. Effect of Temperature on Bubble Diameter in Irradiated Boron Carbide.

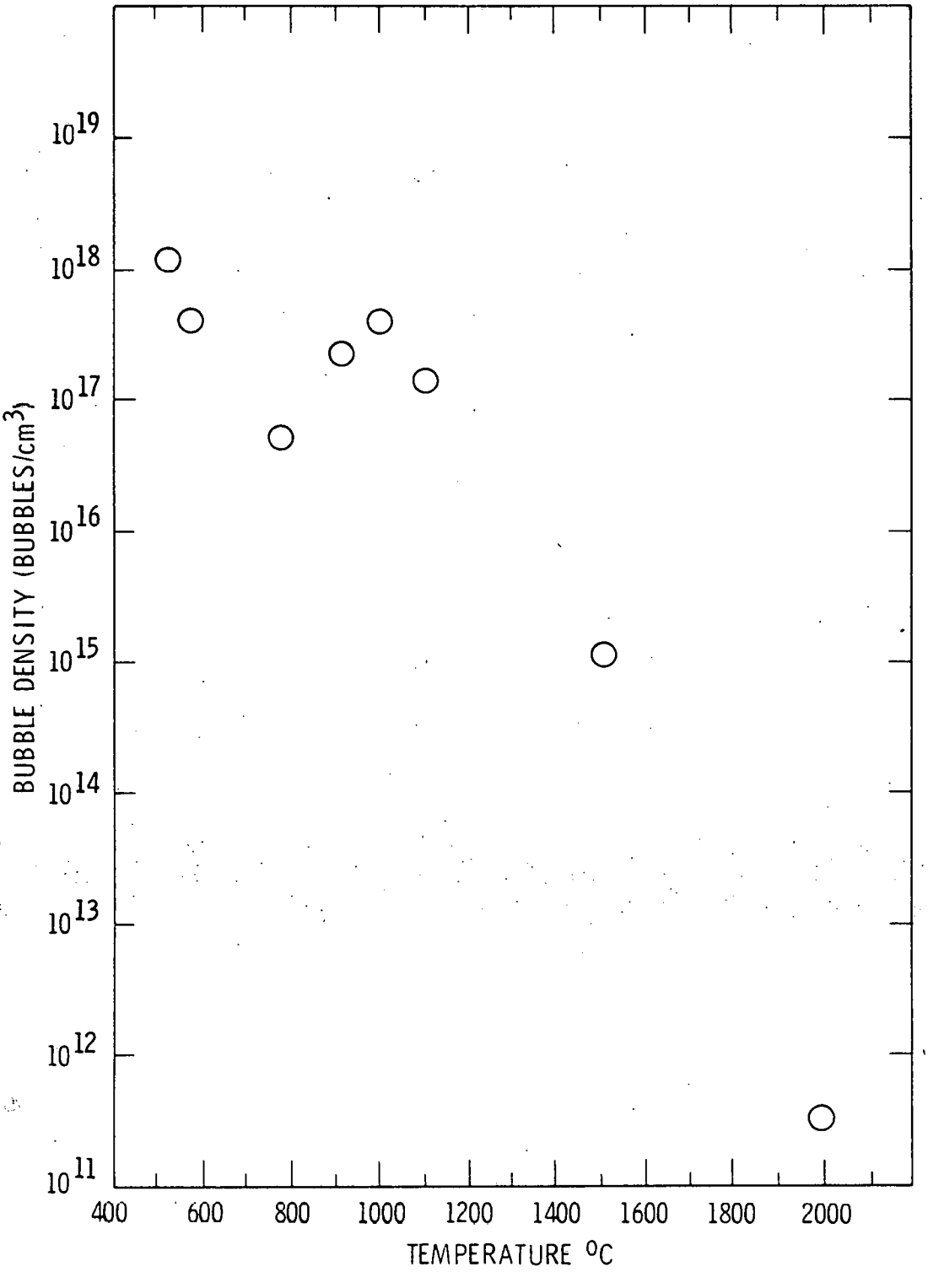

HEDL 7903-043.1

FIGURE 18. Effect of Temperature on Bubble Density in Irradiated Boron Carbide.

Helium production in boron carbide is a consequence of the ^{10}B burnup reaction which forms an alpha particle. As a result of this reaction, helium atoms are expected to be generated evenly throughout the crystallites.

Nucleation of gas bubbles in nuclear fuel may be either homogeneous or heterogeneous. Homogeneous nucleation consists of the formation of stable nuclei by chance encounters of helium atoms. Homogeneous nucleation, consequently, results in high concentration of bubble sites distributed evenly throughout the lattice with very short diffusion distances between the point of helium creation and the location of a cluster. Homogeneous nucleation theories are quite complex and do not allow rational simplification or generalization, but they tend to predict that the nucleation rate would decrease at higher temperatures.[15]

Heterogeneous nucleation relates to the formation of a stable bubble nucleus near a localized disparity in the lattice, i.e., dislocations, grain boundaries, second phase, etc. At low temperatures, so many homogeneously nucleated bubble sites are available that diffusion of helium atoms to heterogeneous sites in the bubble growth stage is not necessary. But at higher temperatures, the reduction in homogeneously nucleated sites requires that helium migrate to bubbles formed on heterogeneous sites. Also at higher temperatures, it is anticipated that there is a greater mobility and the helium atoms could traverse the long distances required to reach the heterogeneous sites.

Bubble nucleation in boron carbide appeared to be high and homogeneous at low temperatures and low and heterogeneous at high temperatures. This temperature effect on helium bubbles in boron carbide is consistent with the theoretical expectations derived from nuclear fuel nucleation models.[15] In these high temperature boron carbide samples, the obvious proximity of bubbles to dislocations, grain boundaries and twins is indicative of heterogeneous nucleation.

The simplest bubble growth mechanism is the result of diffusive flow of individual gas atoms (or defects) to the nucleated bubbles. The driving force for such a flow is the high concentration of helium atoms within the lattice in relation to the solubility limit of helium in boron carbide. The presence of helium sinks (bubbles) offers a mechanism of reducing the free energy of the nonequilibrium situation. This type of growth may, in fact, be the basis for much of the observed in-reactor bubble growth in boron carbide.

The bubble growth noted in postirradiation annealing experiments at high temperatures obviously must have incorporated some of the more complex mechanisms. Resolution, bubble migration or coalescence were necessary in order to make the transition from the small, high density bubbles to the large, low density bubbles that were present after annealing. In-reactor, there was no indication that pre-existing, small, homogeneous bubbles ever existed in order for these mechanisms to operate. Hence, it appears that the bubble growth mechanism in-reactor may be significantly different than ex-reactor. However, the ultimate product in each case (large, faceted bubbles) was obviously similar for in-reactor and annealing investigations (See Figures 2 and 6-12).

In the intermediate temperature range (900 to 1100°C) it was observed that there was a reduction in the density of small bubbles near larger bubbles and grain boundaries. This observation was taken to indicate a localized depletion of helium atoms in the matrix by the major diffusional sink, i.e. the large helium bubble or grain boundary, such that the chemical potential available for nucleus formation and growth in that vicinity was reduced.

Conclusion

The density, shape, and size of helium bubbles in boron carbide has been found to change dramatically when the irradiation temperature was varied from 500 to 2000°C.

The results indicated that homogeneous nucleation mechanisms predominated at low temperature while heterogeneous nucleation mechanisms existed at high temperatures. These results will be utilized in the development of correlations for boron carbide swelling and gas release.

REFERENCES

1. W. V. Cummings, J. J. Laidler, D. E. Mahagin, and B. Mastel, "Microstructure of Fast-Reactor-Irradiated Boron Carbide," Trans. ANS, 15 [2] pp. 742, 1972.

2. G. L. Copeland, R. G. Donnelly, and W. R. Martin, "Irradiation Behavior of Boron Carbide," Nucl. Tech., 16 [1], pp. 226-37, 1972.

3. A. Jostsons and C. K. H. DuBose, "Microstructure of Boron Carbide After Fast Neutron Irradiation," J. Nucl. Mat., 44 [1], pp. 91-95, 1972.

4. K. H. G. Ashbee, "Defects in Boron Carbide, Before and After Neutron Irradiation," Acta. Met., 19 [10], pp. 1070-85, 1971.

5. A. Jostsons, C. K. H. DuBose, G. L. Copeland, and J. O. Stiegler, "Defect Structure of Neutron-Irradiated Boron Carbide," J. Nucl. Mat., 49 [2], pp. 136-50, 1973.

6. G. W. Hollenberg and W. V. Cummings, "Effect of Fast Neutron Irradiation on the Structure of Boron Carbide," J. Am. Cer. Soc., 60, pp. 520-525, 1977.

7. W. V. Cummings and D. E. Mahagin, "Crystallographic Changes in Fast-Reactor-Irradiated Boron Carbide," Trans. ANS, 17, pp. 187-88, 1973.

8. D. E. Mahagin, "Annealing Behavior of Porosity in Irradiated Boron Carbide," Ph.D. Thesis, Washington State University, 1974.

9. F. W. Wiffen and E. E. Bloom, "Swelling and Microstructural Changes in Type 316 Stainless Steel Irradiated Under Simulated CTR Conditions," CONF-750989, Radiation Effects and Tritium Technology for Fusion Reactors, 1976.

10. D. J. Mazey and R. S. Nelson, "The Influence of Preinjected Helium on Void Swelling in Ion-Irradiated Stainless Steels," CONF-750989, Radiation Effects and Tritium Technology for Fusion Reactors, 1976.

11. C. J. Acker, R. R. Vanderort, W. L. Barmore, and N. M. Scanlan, "TEM Investigation of Brittle Fracture of Niobium with Helium by the Tritium Trick," 1978 International Metallographic Exhibit, Edited by C. K. H. DuBose, Published by ASM, Cleveland, Ohio, 1978.

12. J. A. Basmajian and A. L. Pitner, "Helium Retention and Its Effects on Boron Carbide Irradiated in a Fast Reactor," Am. Cer. Soc. Bull., 54 [9], pp. 826, 1975.

13. J. E. Hilliard, "The Counting and Sizing of Particles in Transmission Electron Microscopy," Trans. AIME., 224, pp. 906, 1962.

14. F. J. Homan, "Performance Modeling of Neutron Absorbers," Nucl. Tech., 16, pp. 216, 1972.

REFERENCES (cont'd)

15. D. R. Olander, "Fundamental Aspects of Nuclear Reactor Fuel Elements," University of California, Berkeley, Calif. TID-26711-P1, 1976.

16, B. L. Eyre and P. Bullough, "The Formation of Gas Bubbles in a Nonuniform Temperature Environment," J. Nucl. Mat. 26, pp. 249, 1960